

# Neutron Stars in the Laboratory

Condensed Matter and Astrophysics Seminar

Northwestern  
Nov 9, 2017

Vanessa Gruber, McGill University  
[vanessa.gruber@mcgill.ca](mailto:vanessa.gruber@mcgill.ca)



# Contents

- 1 Neutron Stars in a Nutshell**
- 2 Superfluids**
- 3 Superconductors**
- 4 Laboratory Neutron Star Analogues**

- 1 Neutron Stars in a Nutshell**
- 2 Superfluids**
- 3 Superconductors**
- 4 Laboratory Neutron Star Analogues**

- Neutron stars are one type of **compact remnant**, created during the final stages of stellar evolution.
- When a massive star of  $\sim 8 - 30 M_{\odot}$  runs out of fuel, it collapses under its own gravitational attraction and explodes in a **supernova**.
- These explosions are some of the **most energetic events** in the Universe, releasing  $\sim 10^{51}$  erg.
- During collapse, **electron captures** ( $p + e^- \rightarrow n + \nu_e$ ) produce neutrons.

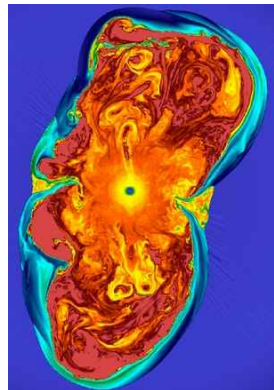
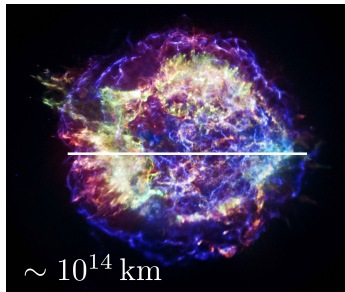


Figure 1: Snapshot of 3D core-collapse supernova simulation (Mösta et al., 2014).



$\sim 10^{14}$  km

Figure 2: Chandra X-ray observation of the Cassiopeia A supernova remnant, which hosts the youngest known neutron star.

- Neutron stars typically have radii between **10 – 15 km** and masses of  **$1.4 – 2 M_{\odot}$** , resulting in mass densities up to  $\rho \simeq 10^{15} \text{ g cm}^{-3}$ .



- Masses and radii are highly dependent on the **equation of state** of nuclear matter, one of the key **unknowns** of neutron star physics.

# Neutron stars

# Pulsars

- Neutron stars have high magnetic fields between  $10^8 - 10^{15}$  G. The Earth's magnetic field is  $\sim 0.5$  G.
- Because rotation and magnetic axes are misaligned, neutron stars emit beams like a **lighthouse**. We observe these regular radio pulses on Earth (Hewish et al., 1968).

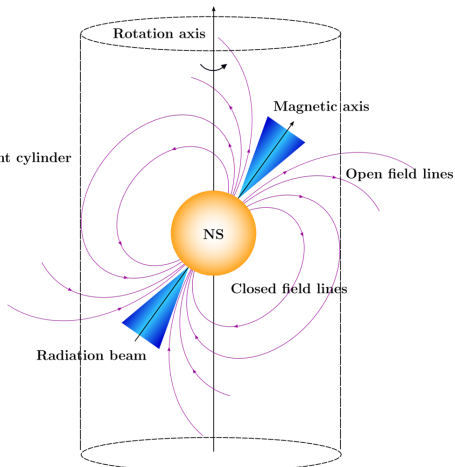
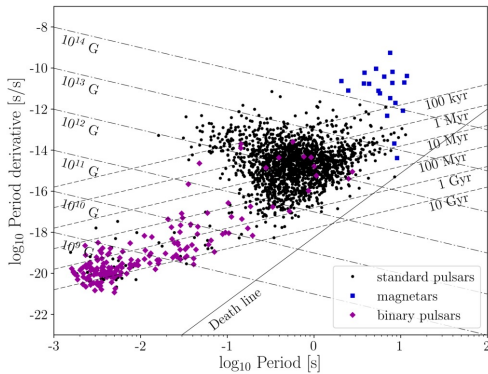


Figure 3: Sketch of the neutron star exterior.

- The  $P\dot{P}$ -diagram is a great diagnostic tool to analyse pulsar physics. Characteristic ages and magnetic field strengths are estimated as

$$\tau_c \sim 0.5 P\dot{P}^{-1}, \quad B \sim 3.2 \times 10^{19} (P\dot{P})^{1/2} \text{ G}. \quad (1)$$



**Figure 4:**  $P\dot{P}$ -diagram for  $\sim 2500$  known radio pulsars from the ATNF pulsar catalogue, which can be found at <http://www.atnf.csiro.au/people/pulsar/psrcat/>. Different classes of neutron stars are highlighted including standard rotation-powered pulsars, magnetars and binary pulsars.

- The interior structure is complex and influenced by the (unknown) equation of state. However, there is a **canonical understanding**.
- After  $\sim 10^4$  years neutron stars are in equilibrium and have temperatures of  $10^6 - 10^8$  K. They are composed of **distinct layers**.
- For our purposes we separate neutron stars into a **solid crust** and a **fluid core**.

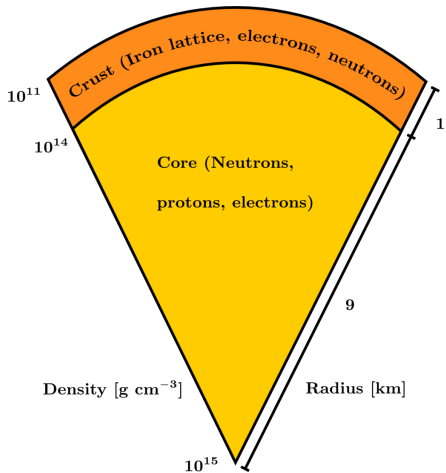


Figure 5: Sketch of the neutron star interior.

- Neutron stars are hot compared to low-temperature experiments on Earth, but cold in terms of their nuclear physics (Migdal, 1959).
- Neutrons and protons are **fermions** that can become unstable to **Cooper pair** formation due to an attractive contribution to the nucleon-nucleon interaction potential.
- Pairing process is described within the standard microscopic **BCS** theory of superconductivity (Bardeen, Cooper & Schrieffer, 1957).
- Compare the equilibrium to the nucleons' **Fermi temperature**:

$$T_F = k_B^{-1} E_F \sim 10^{12} \text{ K} \gg 10^6 - 10^8 \text{ K}. \quad (2)$$

**Neutron star matter is strongly influenced by quantum mechanics!**

- Detailed BCS calculations provide the pairing gaps  $\Delta$ , which are associated with the **critical temperatures**  $T_c$  for the superfluid and superconducting phase transitions.

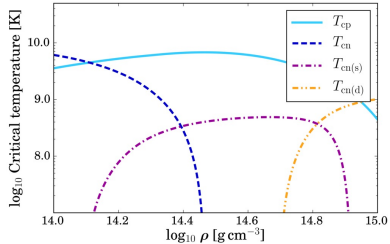
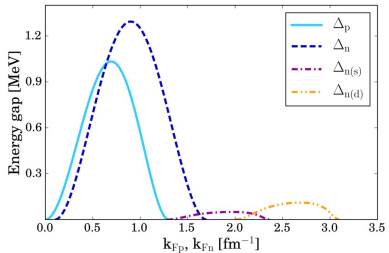


Figure 6: Left: Parametrised proton (singlet) and neutron (singlet, triplet) energy gaps as a function of Fermi wave numbers (Ho, Glampedakis & Andersson, 2012). Right: Critical temperatures of superconductivity/superfluidity as a function of the neutron star density. The values are computed for the NRAPR equation of state (Steiner et al., 2005; Chamel, 2008).

1 Neutron Stars in a Nutshell

2 Superfluids

3 Superconductors

4 Laboratory Neutron Star Analogues

- Superfluids flow **without viscosity**, while superconductors have vanishing electrical conductivity and exhibit **Meissner effect**.
- Both states involve large numbers of particles condensed into the same quantum state, characteristic for **macroscopic quantum phenomena**.
- Most of our understanding of superfluidity and superconductivity in neutron stars originates from **laboratory counterparts**.

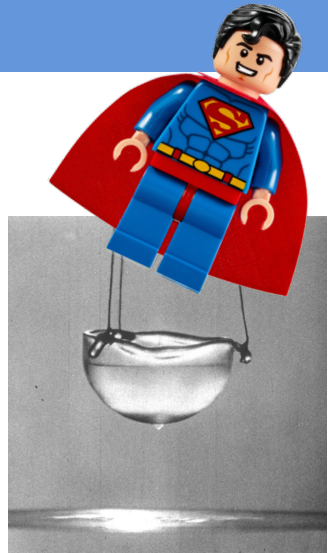


Figure 7: Superfluid helium creeps up the walls to eventually empty the bucket.

# Superfluids

## Two-fluid phenomenology

- At low temperatures helium-4 does **not solidify**. Instead at the **2.171 K Lambda point** it enters a new fluid phase (Kapitza, 1938; Allen & Misener, 1938).

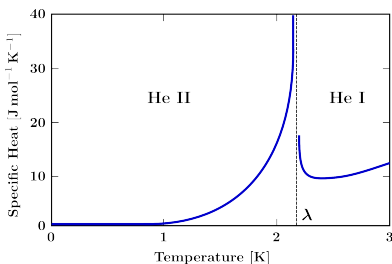
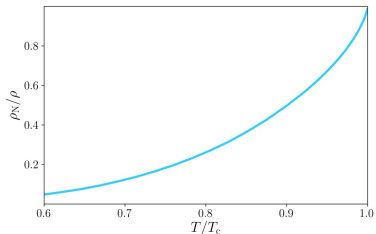


Figure 8: Heat capacity behaviour at superfluid transition in helium-4 resembles the Greek letter  $\lambda$ .

Figure 9: Normal fluid fraction in helium II (Barenghi, Donnelly & Vinen, 1983).



- Behaviour below  $T_c$  is explained by a **two-fluid model**: an inviscid (superfluid features) and a normal component (viscous properties, heat transport) coexist (Tisza, 1938; Landau, 1941).

- The inviscid component is characterised by a **macroscopic wave function**  $\Psi = \Psi_0 e^{i\varphi}$  that satisfies the Schrödinger equation. Using the standard formalism one can determine a **superfluid velocity**

$$v_s \equiv \frac{\mathbf{j}_s}{\rho_s} = \frac{\hbar}{m_c} \nabla \varphi, \quad \Rightarrow \quad \boxed{\boldsymbol{\omega} \equiv \nabla \times \mathbf{v}_s = 0}. \quad (3)$$



Figure 10: Envisage vortices as tiny, rapidly rotating tornadoes.

- Superflow is **irrotational** and does not allow classical rotation. Different to a viscous fluid, a superfluid inside a rotating container minimises its energy by forming a **regular vortex array**.
- Each vortex has a velocity profile  $v_s \propto 1/r$  and carries a **quantum of circulation**

$$\kappa = \frac{\hbar}{2m} \approx 2.0 \times 10^{-3} \text{ cm}^2 \text{ s}^{-1}. \quad (4)$$

- The vortices arrange themselves in a **hexagonal array** (Abrikosov, 1957) and their circulation mimics solid-body rotation on macroscopic length scales. The **vortex area density**  $\mathcal{N}_v$  is

$$\omega = 2\Omega = \mathcal{N}_v \kappa \hat{z}, \quad \rightarrow \quad \mathcal{N}_v \approx 6.3 \times 10^5 \left( \frac{P}{10 \text{ ms}} \right)^{-1} \text{ cm}^{-2}. \quad (5)$$

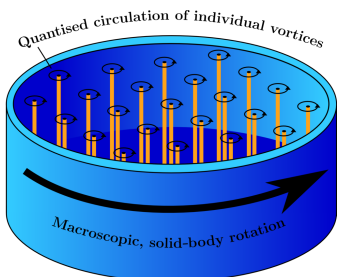


Figure 11: Vortex array of a rotating superfluid mimics solid-body rotation.

- For a regular array, the **intervortex distance** is given by  $d_v \simeq \mathcal{N}_v^{-1/2}$ :

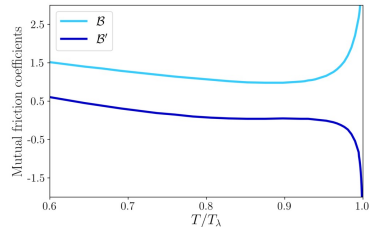
$$d_v \approx 1.3 \times 10^{-3} \left( \frac{P}{10 \text{ ms}} \right)^{1/2} \text{ cm}. \quad (6)$$

- A change in angular momentum is achieved by creating (spin-up) or destroying (spin-down) vortices.

- The vortices can interact with the viscous fluid component causing dissipation. This is referred to as **mutual friction** and influences lab systems and neutron stars (Hall & Vinen, 1956, e.g.).
- For a system rotating at  $\Omega = \Omega \hat{\Omega}$ , the **vortex-averaged** drag force is

$$\mathbf{F}_{\text{mf}} = \mathcal{B} \frac{\rho_S \rho_N}{\rho} \hat{\Omega} \times [\Omega \times (\mathbf{v}_S - \mathbf{v}_N)] + \mathcal{B}' \frac{\rho_S \rho_N}{\rho} \Omega \times (\mathbf{v}_S - \mathbf{v}_N). \quad (7)$$

- The **dimensionless parameters**  $\mathcal{B}$  and  $\mathcal{B}'$  reflect the strength of the mutual friction and can be measured in helium (Barenghi, Donnelly & Vinen, 1983) and calculated for neutron stars (Alpar, Langer & Sauls, 1984).

Figure 12:  $\mathcal{B}$  and  $\mathcal{B}'$  in helium II.

**1** Neutron Stars in a Nutshell

**2** Superfluids

**3** Superconductors

**4** Laboratory Neutron Star Analogues

- Superconductors are often studied by their response to an external field, providing information about the internal magnetisation. **Flux expulsion** (the Meissner effect) was first described within the phenomenological **London model** (London & London, 1935)

$$\lambda^2 \nabla^2 \mathbf{B} = \mathbf{B}, \quad \text{where} \quad \lambda \equiv \left( \frac{m_c c^2}{4\pi n_c q^2} \right)^{1/2}. \quad (8)$$

- The solution for  $\mathbf{B}$  decays exponentially: the **penetration depth**  $\lambda$  determines the thickness of the surface supercurrent sheet.
- The London model has a **microscopic origin**. As in the superfluid case, quantum mechanics allows us to derive a supercurrent density

$$\mathbf{j}_s = -\frac{q^2}{m_c c} n_c \mathbf{A}. \quad (9)$$

- Due to their distinct responses to an applied magnetic field, superconductors can be separated into **type-I** and **type-II** media.

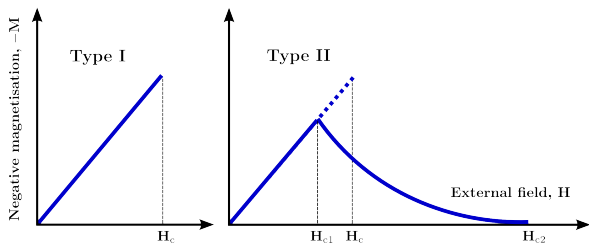


Figure 13: Magnetisation curves for a type-I (left) and type-II (right) medium with the same  $H_c$ .

- The **critical field**  $H_c$  is related to the energy difference between the normal and superconducting state, i.e. the condensation energy.

- For  $H_{c1} \leq H \leq H_{c2}$ , Meissner state does not break down abruptly but flux enters continuously through fluxtubes (Abrikosov, 1957).
- Each fluxtube has a profile  $v_S \propto e^{-r/\lambda}$  and carries a **flux quantum**

$$\phi_0 = \frac{hc}{2e} \approx 2.1 \times 10^{-7} \text{ G cm}^2. \quad (10)$$

- All flux quanta add up to the total magnetic flux. The **averaged magnetic induction** is related to the fluxtube area density  $\mathcal{N}_{ft}$  via

$$B = \mathcal{N}_{ft} \phi_0, \quad \rightarrow \quad \mathcal{N}_{ft} \approx 4.8 \times 10^{18} \left( \frac{B}{10^{12} \text{ G}} \right) \text{ cm}^{-2}. \quad (11)$$

- The typical **interfluxtube distance** is given by  $d_{ft} \simeq \mathcal{N}_{ft}^{-1/2}$  with

$$d_{ft} \approx 4.6 \times 10^{-10} \left( \frac{B}{10^{12} \text{ G}} \right)^{1/2} \text{ cm}. \quad (12)$$

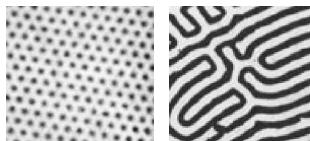


Figure 14: Superconducting states.

- Baym, Pethick & Pines (1969) argue that due to high conductivity, magnetic flux cannot be expelled from the interior and flux has to be retained in a type-II or intermediate type-I state. This implies that neutron stars do not exhibit Meissner effect and are **metastable**.

- The exact phase depends on the characteristic lengthscales involved:

$$\kappa \approx 3.3 \left( \frac{m_p^*}{m} \right)^{3/2} \left( \frac{\rho}{10^{14} \text{ g cm}^{-3}} \right)^{5/6} \left( \frac{x_p}{0.05} \right)^{5/6} \left( \frac{T_{cp}}{10^9 \text{ K}} \right) > \frac{1}{\sqrt{2}}. \quad (13)$$

- The outer core is expected to be in a type-II state. **Field evolution** is related to the motion of fluxtubes and mechanisms affecting them (Muslimov & Tsygan, 1985; Gruber et al., 2015, e.g.).

- Macroscopic **Euler equations** for superfluid neutrons and charged fluid in zero-temperature limit (Glampedakis, Andersson & Samuelsson, 2011)

$$(\partial_t + v_n^j \nabla_j) [v_n^i + \varepsilon_n w_{np}^i] + \nabla^i \tilde{\Phi}_n + \varepsilon_n w_{pn}^j \nabla^i v_j^n = f_{mf}^i + f_{mag,n}^i, \quad (14)$$

$$(\partial_t + v_p^j \nabla_j) [v_p^i + \varepsilon_p w_{pn}^i] + \nabla^i \tilde{\Phi}_p + \varepsilon_p w_{np}^j \nabla^i v_j^p = -\frac{n_n}{n_p} f_{mf}^i + f_{mag,p}^i, \quad (15)$$

with  $w_{xy}^i \equiv v_x^i - v_y^i$ . Modified by **new force terms**,  $f_{mf}^i$  and  $f_{mag,x}^i$ , due to vortices/fluxtubes and **entrainment**,  $\varepsilon_x$  (Andreev & Bashkin, 1975).

- Supplemented by **continuity equations** and **Poisson's equation**

$$\partial_t n_x + \nabla_i (n_x v_x^i) = 0, \quad \nabla^2 \Phi = 4\pi G \rho, \quad (16)$$

and an evolution equation for the magnetic induction  $B$ .

- 1 Neutron Stars in a Nutshell**
- 2 Superfluids**
- 3 Superconductors**
- 4 Laboratory Neutron Star Analogues**

- The interior of neutron stars contains distinct superfluid components and theoretical models crucially depend on the understanding of their laboratory counterparts.
- It is **not possible to replicate** the extreme conditions present in neutron stars. However, we could specifically aim to use known laboratory analogues that are easy to manipulate in order to recreate and **study specific neutron star characteristics**. This way we can learn something about the physics of their interiors.
- For a comprehensive discussion of different options see Graber, Andersson & Hogg (2017).

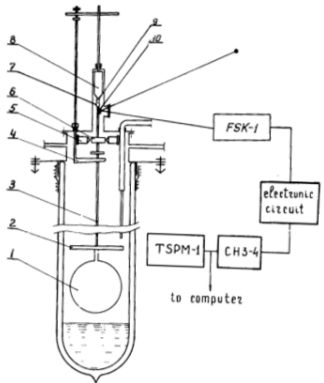


Figure 15: Schematic setup of the helium II spin-up experiments (Tsakadze & Tsakadze, 1980).

- First (and only) **systematic analysis** of rotating helium II by Tsakadze & Tsakadze (1980), shortly after first observations of **glitches** in the Vela and Crab pulsar.
- Validate presence of superfluid components in neutron stars by measuring **relaxation timescales** after initial changes in the container's rotation.
- Performed for various temperatures, vessel configurations and rotational properties.
- Model comparison is hard (Reisenegger, 1993; van Eysden & Melatos, 2011).

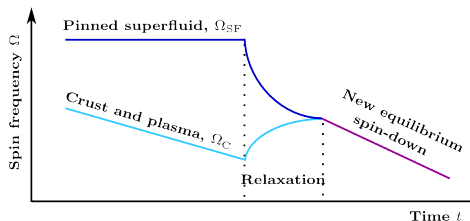


Figure 16: Sketch of an idealised neutron star glitch.

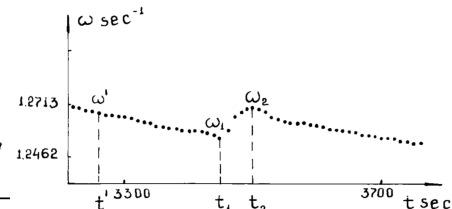


Figure 17: Measurement of a laboratory glitch.

- Glitches are **sudden spin-ups** that interrupt the pulsar spin-down.  
Spontaneous acceleration also observed in rotating helium II.
- Dynamics well explained by a simple **two-component model**.
- However, the mechanism that causes coupling between crust and the pinned superfluid is not known → study with helium II.

- Helium-3 becomes superfluid below 3 mK. The transition is different to bosonic helium II because helium-3 atoms are fermions and have to form **Cooper-pairs** as expected for the neutron star interior.
- The pairing occurs in a spin-triplet,  $p$ -wave state: the Cooper pairs have internal structure resulting in **3 superfluid phases** (Vollhardt, 1998).
- **B-phase** behaves similar to helium II.
- **A-phase** exhibits anisotropic behaviour and can form unusual vortex structures.

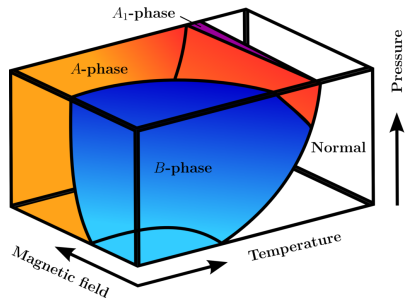


Figure 18: Schematic phase diagram of helium-3.

- It is not understood how **interfaces** influence the neutron star dynamics → **crust-core transition** between two superfluids??

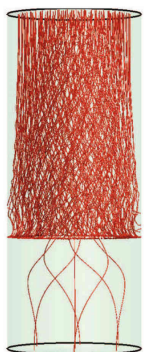
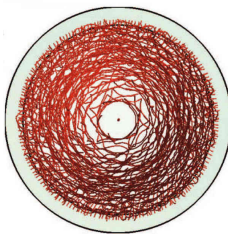


Figure 19: Vortex-line simulation for spin-down of two-phase helium-3 (Walmsley et al., 2011).

- Study vortices across an interface with rotating **two-phase samples** (different  $\beta$ ,  $\beta'$ ) using NMR measurements and modern vortex-line simulations (Walmsley et al., 2011).
- Interface strongly modifies dynamics:
  - ▶ **Vortex sheet** formation
  - ▶ **Vortex tangle** forms in  $B$ -phase, reconnections increase dissipation
  - ▶ **Differential rotation**
- Interface can become unstable to Kelvin-Helmholtz instability (Finne et al., 2006).

- A BEC of **weakly-interacting bosons** was first realised cooling Rubidum atoms to  $T \sim nK$  (Anderson et al., 1995; Davis et al., 1995).
- **Superfluid transition** and vortex formation are present (Matthews et al., 1999; Madison et al., 2000).
- Similar properties to helium II as BECs are governed by a generalised Schrödinger equation, the **Gross-Pitaevskii equation**.
- **Absorption imaging** of clouds is a great tool to study behaviour of individual vortices.

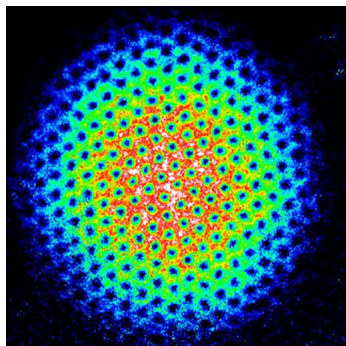


Figure 20: Vortex array in a rotating, dilute BEC of Rubidium atoms (Engels et al., 2002).

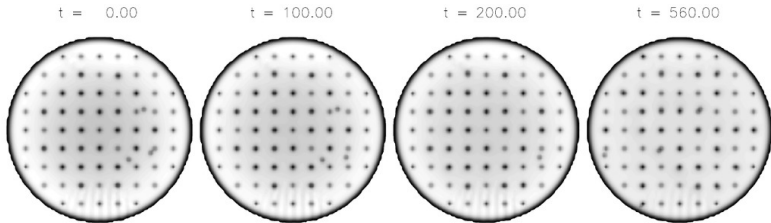


Figure 21: Snapshots of superfluid density during the spin-down of a BEC (Warszawski & Melatos, 2012).

- Time evolution of the Gross-Pitaevskii equation describes BEC **vortex motion** → use this approach to study the pinned **crustal superfluid** in neutron stars (Warszawski & Melatos, 2012).
- Collective vortex motion in the presence of pinning potential can cause **glitch-like events** → study the unknown trigger.

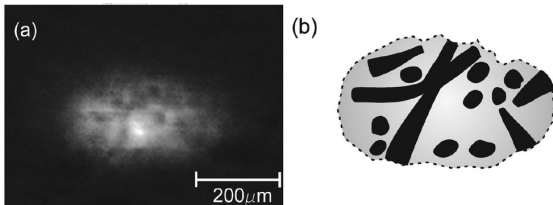


Figure 22: BEC vortex tangle: snapshot of atomic density and corresponding sketch (Henn et al., 2009).

- Chaotic superflow is referred to as **quantum turbulence** (Vinen & Niemela, 2002): large scale features are similar to classical turbulence, but behaviour differs on small-scales → **take pictures** of this.
- Turbulence in neutron stars would alter the dissipation, which affects many macroscopic phenomena such as the post-glitch relaxation or oscillation damping → study **new phenomena**.

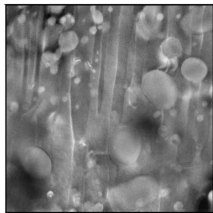


Figure 23: 3D STEM tomogram with  $\sim 70$  pinning sites (Ortalan et al., 2009).

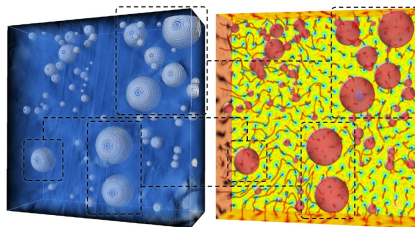


Figure 24: Modelled fluxtube motion. Colour reflects order parameter (Sadovskyy et al., 2016).

- Experimental data and modern calculations complement each other: Determine **fluxtube motion** in a **realistic pinning landscape** by numerically solving time-dependent Ginzburg-Landau equations.
- Account for pinning defects, fluxtube flexibility, long-range fluxtube repulsion, fluxtube cutting and reconnections.

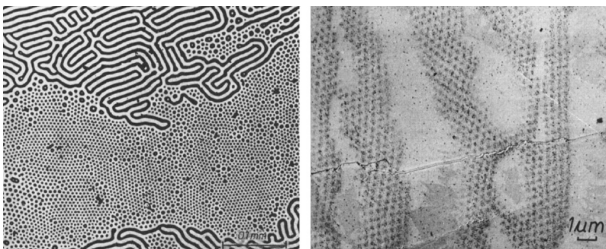


Figure 25: Intermediate state of type-I and type-II phases (Brandt & Essmann, 1987; Essmann, 1971).

- Our understanding of **macroscopic superconductivity** in neutron stars is based on time-independent equilibrium considerations. It is unclear what happens in details as the star cools below  $T_c$ .
- One aspect is that the **transition temperature** is not constant throughout the neutron star's interior but **density-dependent**.

- The superconducting region expands inside the star as it cools down. Its size depends on the equation of state and pairing gap model.

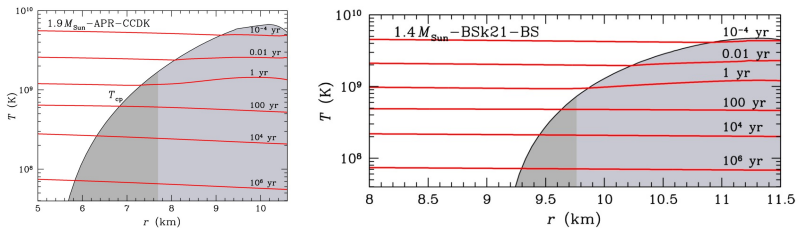


Figure 26: Two gap models and two EoSs plus cooling curves accounting for modified Urca and  $\rho$  Cooper pair cooling but neglecting neutron superfluidity (Ho, Andersson & Graber (2017) submitted).

- Flux can only be expelled if cooling proceeds slower than nucleation. Alternatively compare **lengthscales** of cooling and flux expulsion.

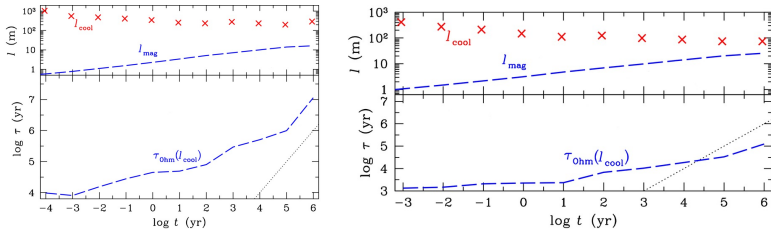


Figure 27: Lengthscale comparison for  $B_0/H_c \sim 10^{-5}$  (Ho, Andersson & Gruber (2017) submitted).

- For **broad gap models**, cooling is always faster than flux expulsion. Only for **very narrow gaps** and low magnetic fields  $B_0 \sim 10^{10}$  G it might be possible to create flux-free spherical shell after  $t \sim 10^5$  yr.
- Experiments could help to better understand the small-scale **dynamics** of the phase transition and the resulting flux distribution.

# Conclusions

- Neutron stars are born when massive stars run out of fuel and explode in **supernovae**. They contain a mass comparable to the Sun's within a radius of about ten kilometres and exhibit **extreme conditions**. Their interior is very difficult to probe.
- Superfluids and superconductors have the special ability to **flow without friction**, leading to many surprising experimental results. This behaviour is a direct consequence of **quantum mechanics**. However, on large scales hydrodynamical descriptions are available to capture their behaviour.

There are many exciting ways to combine both fields of research and probe the dynamics of the neutron star interior with superfluid/superconducting laboratory experiments!!

- Superfluidity and superconductivity are usually not accounted for in **gravitational wave signal** modelling as the effects of macroscopic condensates are generally believed to be negligible.
- It has been suggested that **tidal disruption** during the late inspiral could dynamically couple to neutron star oscillations. If this is true than superfluidity/superconductivity could modify wave forms.

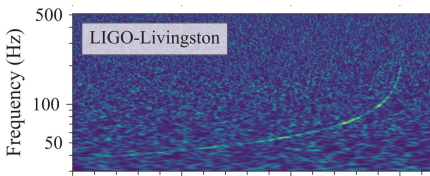


Figure 28: Time-frequency representation of GW170817 (Abbott et al., 2017).

- Quantum states can only be present if stars are cold enough. Not clear how parameters like **temperature, conductivities and viscosities** evolve during the merger.

- Isolated neutron stars are likely to exhibit **non-spherical dynamical changes** in the interior fluid, which would result in the emission of gravitational waves (small amplitude).
- Interesting oscillations are the **r-modes** (inertial modes in rotating objects dominated by Coriolis force), because they are susceptible to the **CFS (Chandrasekhar-Friedman-Schutz) instability**.
- They can be prograde in inertial but retrograde in rotating frame, so that GW emission does not damp but increase amplitudes. Detailed physics will depend on presence of quantum condensates.

Figure 29: Oscillation seen by inertial (left) and rotating (right) observer (animation by Ben Owen).

- Mutual friction coefficients cannot be directly measured  $\Rightarrow$  **calculate coupling physics** for a single vortex then average for the entire array.  
Mesoscopic dimensionless drag,  $\mathcal{R}$ , is related to  $\mathcal{B}$  and  $\mathcal{B}'$  via

$$\mathcal{B} = \frac{\mathcal{R}}{1 + \mathcal{R}^2}, \quad \mathcal{B}' = \frac{\mathcal{R}^2}{1 + \mathcal{R}^2}. \quad (17)$$

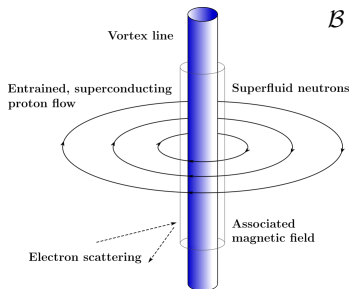
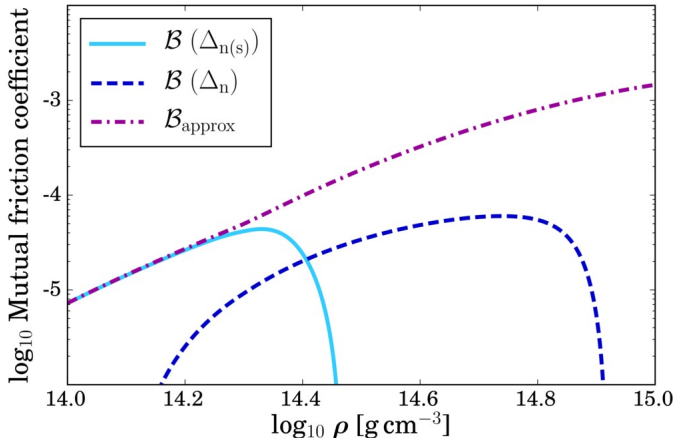
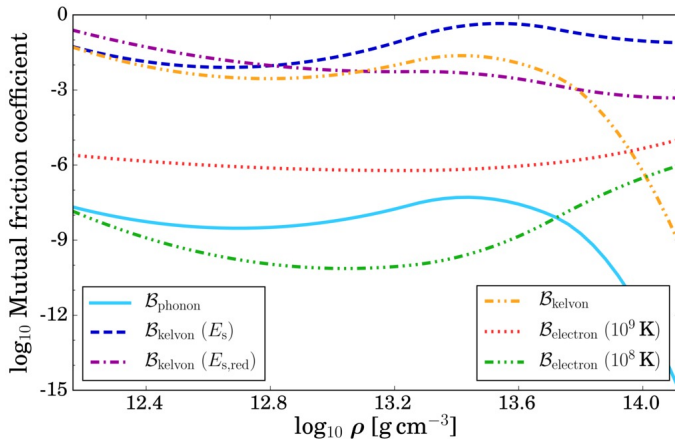


Figure 30: Canonical mutual friction coupling in neutron star core.

- **Core:** electron scattering off vortex magnetic field,  $\mathcal{B} \sim 10^{-5}$ .
- **Crust:** several mechanisms possible,  $\mathcal{B} \sim 10^{-2}$  (kelvon excitation) or  $\mathcal{B} \sim 10^{-8}$  (phonon excitation).





$$\lambda_* \approx 1.3 \times 10^{-11} \left( \frac{m_p^*}{m} \right)^{1/2} \rho_{14}^{-1/2} \left( \frac{x_p}{0.05} \right)^{-1/2} \text{ cm}, \quad (18)$$

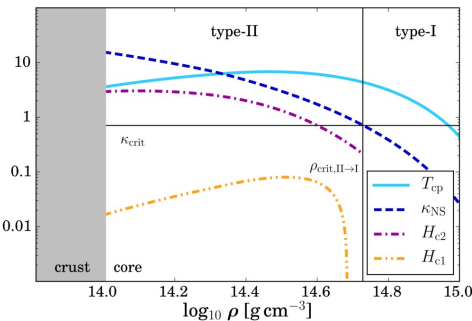
$$\xi_p \approx 3.9 \times 10^{-12} \left( \frac{m}{m_p^*} \right) \rho_{14}^{1/3} \left( \frac{x_p}{0.05} \right)^{1/3} \left( \frac{10^9 \text{ K}}{T_{cp}} \right) \text{ cm}, \quad (19)$$

$$\xi_n \approx 1.5 \times 10^{-11} (1 - x_p)^{1/3} \left( \frac{m}{m_n^*} \right) \rho_{14}^{1/3} \left( \frac{10^9 \text{ K}}{T_{cn}} \right) \text{ cm}, \quad (20)$$

$$H_{c1} \approx 1.9 \times 10^{14} \left( \frac{m}{m_p^*} \right) \rho_{14} \left( \frac{x_p}{0.05} \right) \text{ G}, \quad (21)$$

$$H_{c2} \approx 2.1 \times 10^{15} \left( \frac{m_p^*}{m} \right)^2 \rho_{14}^{-2/3} \left( \frac{x_p}{0.05} \right)^{-2/3} \left( \frac{T_{cp}}{10^9 \text{ K}} \right)^2 \text{ G}. \quad (22)$$

**Figure 31:** Density-dependent parameters of NS superconductivity calculated for the NRAPR effective equation of state (Steiner et al., 2005).  $T_{\text{cp}}$  is obtained from Ho, Glampedakis & Andersson (2012).



- Parameters of superconductivity are dependent on the neutron star density, i.e. the **equation of state**.
- At higher densities one eventually has  $\kappa < 1/\sqrt{2}$ , so that the type-II state should transition into a **type-I state**. The critical density is

$$\rho_{\text{crit},\text{II} \rightarrow \text{I}} \approx 6.4 \times 10^{14} \left( \frac{m_p^*}{m} \right)^{-\frac{9}{5}} \left( \frac{0.05}{x_p} \right) \left( \frac{T_{\text{cp}}}{10^9 \text{ K}} \right)^{-\frac{6}{5}} \text{ g cm}^{-3}. \quad (23)$$

- Time to expel magnetic flux a distance  $L$  from a normal conductor is

$$\tau_{\text{nucl}} = \frac{L^2}{D} \frac{B_0}{2H_c} = \tau_{\text{ohm}} \frac{B_0}{2H_c} \sim 10^{10} \left( \frac{\tau_{\text{Ohm}}}{10^{13} \text{ yr}} \right) \left( \frac{B_0/H_c}{10^{-3}} \right) \text{ yr.} \quad (24)$$

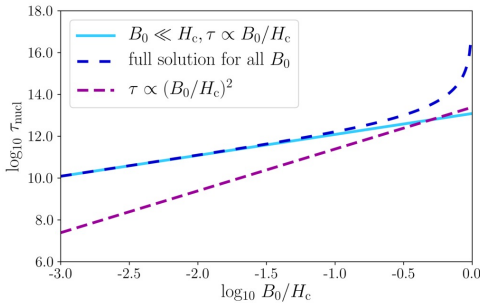


Figure 32: Nucleation timescales as a function of  $B_0/H_c$  for  $\sigma_e = 5.5 \times 10^{28} \text{ s}$  and  $L = 10^6 \text{ cm}$ .

# Appendix

# References |

- Abbott B. P. et al., 2017, Physical Review Letters, 119, 161101
- Abrikosov A. A., 1957, Journal of Physics and Chemistry of Solids, 2, 199
- Allen J. F., Misener A. D., 1938, Nature, 141, 75
- Alpar M. A., Langer S. A., Sauls J. A., 1984, The Astrophysical Journal, 282, 533
- Anderson M. H., Ensher J. R., Matthews M. R., Wieman C. E., Cornell E. A., 1995, Science, 269, 198
- Andreev A. F., Bashkin E. P., 1975, Soviet Physics JETP, 42, 164
- Bardeen J., Cooper L. N., Schrieffer J. R., 1957, Physical Review, 108, 1175
- Barenghi C. F., Donnelly R. J., Vinen W. F., 1983, Journal of Low Temperature Physics, 52, 189
- Baym G., Pethick C. J., Pines D., 1969, Nature, 224, 673
- Brandt E. H., Essmann U., 1987, physica status solidi (b), 144, 13
- Chamel N., 2008, Monthly Notices of the Royal Astronomical Society, 388, 737
- Davis K., Mewes M.-O., Andrews M. R., van Druten N. J., Durfee D. S., Kurn D. M., Ketterle W., 1995, Physical Review Letters, 75, 3969
- Engels P., Coddington I., Haljan P. C., Cornell E. A., 2002, Physical review letters, 89, 100403
- Essmann U., 1971, Physica, 55, 83
- Finne A. P., Eltsov V. B., Hänninen R., Kopnin N. B., Kopu J., Krusius M., Tsubota M., Volovik G. E., 2006, Reports on Progress in Physics, 69, 3157
- Glampedakis K., Andersson N., Samuelsson L., 2011, Monthly Notices of the Royal Astronomical Society, 410, 805
- Graber V., Andersson N., Glampedakis K., Lander S. K., 2015, Monthly Notices of the Royal Astronomical Society, 453, 671

# Appendix

# References II

- Hall H. E., Vinen W. F., 1956, Proceedings of the Royal Society A, 238, 215
- Henn E. A. L., Seman J. A., Roati G., Magalhães K. M. F., Bagnato V. S., 2009, Physical Review Letters, 103, 045301
- Hewish A., Bell S. J., Pilkington J. D. H., Scott P. F., Collins R. A., 1968, Nature, 217, 709
- Ho W. C. G., Andersson N., Gruber V., 2017, submitted to Phys. Rev. C
- Ho W. C. G., Glampedakis K., Andersson N., 2012, Monthly Notices of the Royal Astronomical Society, 422, 2632
- Kapitza P., 1938, Nature, 141, 74
- Landau L. D., 1941, Physical Review, 60, 356
- London F., London H., 1935, Proceedings of the Royal Society A, 149, 71
- Madison K., Chevy F., Wohlleben W., Dalibard J., 2000, Physical Review Letters, 84, 806
- Matthews M. R., Anderson B. P., Haljan P. C., Hall D. S., Wieman C. E., Cornell E. A., 1999, Physical Review Letters, 83, 2498
- Migdal A. B., 1959, Nuclear Physics, 13, 655
- Mösta P. et al., 2014, The Astrophysical Journal, 785, L29
- Muslimov A. G., Tsyan A. I., 1985, Soviet Astronomy Letters, 11, 80
- Ortalan V., Herrera M., Rupich M. W., Browning N. D., 2009, Physica C: Superconductivity and its Applications, 469, 2052
- Reisenegger A., 1993, Journal of Low Temperature Physics, 92, 77
- Sadovskyy I. A., Koshelev A. E., Glatz A., Ortalan V., Rupich M. W., Leroux M., 2016, Physical Review Applied, 5, 014011
- Steiner A. W., Prakash M., Lattimer J. M., Ellis P. J., 2005, Physics reports, 411, 325

- Tsakadze J. S., Tsakadze S. J., 1980, Journal of Low Temperature Physics, 39, 649
- van Eysden C. A., Melatos A., 2011, Journal of Low Temperature Physics, 165, 1
- Vinen W. F., Niemela J. J., 2002, Journal of Low Temperature Physics, 128, 167
- Vollhardt D., 1998, in Pair Correlations in Many-Fermion Systems, Kresin V. Z., ed., Springer US, Boston, MA, pp. 205–220
- Walmsley P. M., Eltsov V. B., Heikkinen P. J., Hosio J. J., Hänninen R., Krusius M., 2011, Physical Review B, 84, 184532
- Warszawski L., Melatos A., 2012, Monthly Notices of the Royal Astronomical Society, 423, 2058